Variability of Targeted Material Thermal Responses to Laser-Induced Heating in Additive Manufacturing

T. I. Zohdi
Department of Mechanical Engineering,
University of California,
Berkeley, CA 94720-1740
e-mail: zohdi@berkeley.edu

N. Castrillon
Department of Mechanical Engineering,
University of California,
Berkeley, CA 94720-1740
e-mail: nicolas.castrillon@berkeley.edu

A widespread use of lasers in additive manufacturing is to induce a given temperature and a phase transformation in materials deposited onto a substrate. For a laser to induce a phase transformation in the material, the power intensity must be sufficiently high to induce melting and, in all cases, stay below a vaporization or burn-off temperature of the target material. Oftentimes, there is variability in the laser input to the target zone. For a process designer, a central question is to determine the uncertainty of the resulting target state, i.e., temperature and state (solid or melted), due to uncertainty in the energy (laser) input. This motivates the present work, which integrates relatively fundamental heat transfer models that describe the thermal effects due to (a) laser irradiation, (b) heat conduction into the surface of deposition, (c) infrared radiation outwards into the surroundings, (d) convection due to an exhaust apparatus to control the cooling of the system, and (e) phase transformations, for a dry Nylon 6 powder as a sample material. One key advantage of this framework is that it is amenable to a sensitivity and uncertainty analysis with respect to any of its parameter inputs. Accordingly, uncertainty quantification studies are also undertaken to ascertain the relationship between variation in laser input to variation in the processed material state. Examples will be presented to illustrate the thermal behavior of the numerical model. Due to its simplicity, this framework is designed to be computationally implemented in a straightforward fashion. The model allows for rapid computation and sensitivity analyses, which are provided as numerical examples. Extensions are also given to include mass transport (losses) due to ablation of the target material.
[DOI: 10.1115/1.4043981]

1 Introduction

One of the primary uses of lasers in manufacturing is to induce a prescribed temperature field within a target material. Specifically, a subset of scenarios of key interest within additive manufacturing (AM) processes involve depositing dry powder-based materials onto a surface and then to heat the targeted material with a laser in order to sinter or melt the target material. Householder [1] pioneered selective laser sintering (SLS) and melting (SLM) in 1979 and then Deckard [2] followed with his work in the mid-1980s. Since then, significant advances have been achieved in the metal-based AM industry as reviewed by Smith et al. [3]. Experimentally, in the realm of materials and microstructure characterization, Voisin et al. [4] studied the detrimental effects of defects and porosity on as-built tensile properties of titanium alloys. Numerically, Wang et al. [5] presented an integrated discrete element method-computational fluid dynamics framework for simulating the deposition of dry powder particles and subsequent phase changes by SLM and electron beam selective melting processes.[1] Additional models and simulation methods for capturing the SLS/SLM processes are presented by Zohdi [6,7]. Selective laser sintering and melting processes are not restricted to metallic powders, however, as it also applies to polymeric [8] and ceramic [9] powder materials, as highlighted by Kinstlinger et al. [10].

In some regimes and related manufacturing processes, a particle mixture may be fluid-like (as opposed to solid-like) and saturated with an interstitial fluid or embedded within a fluid medium. In such cases, the fluid dynamics interaction with the particles can play a major role on the system behavior. This can also involve the evolution of heat. A spatiotemporal discretization can be used to solve coupled fluid-particle systems, by employing finite element, finite difference, or finite volume methods coupled to discrete element methods. There has been ample research that is suited to describe the powder bed dynamics of an SLS process. Oñate et al. [11–13] give an extension of Lagrangian particle finite element methods for fluid interactions at solid–fluid and solid–solid interfaces in soil mechanics; Carbonell et al. [14] describes the adaptation of the particle finite element method to model tool wear for tunneling applications through soil particles; Labra and Oñate [15] employ a finite element mesh to develop an algorithm to efficiently generate high-density packing of spherical particles; Rojek et al. [16] and Rojek [17] present discrete element models for contacting spherical particles; Avci and Wriggers [18] use a coupled descrete element and finite element method for particle-fluid interactions; Leonardi et al. [19] present a Lattice-Boltzmann adaptation for simulating non-Newtonian rheology, free surfaces, and moving boundaries; and Bolintineanu et al. [20] review methods for handling simulations of the dynamics of colloidal suspensions at the mesoscale. All of these studies present techniques to simulate the dynamics of a complex powder particle deposition phase and the rheology of polymer melt flow in an SLS process. Furthermore, work by Salloum et al. [21] represents advances in the optimization of computation cost by providing an efficient data compression/decompression method for storing and transferring large data sets.

In this study, we focus on a thermal model for SLS processing applied to a Nylon 6 polymer. However, this lumped mass model can be useful to simulate any metal, polymeric, or ceramic-based

[1]Additional techniques used in a generalized AM process can include (a) ink jet printing, consists of a pressurized, a heated, and/or a vibrating small orifice to project small ink droplets for deposition on a substrate, and dried by UV light or other means, (b) aerosol jetting, which directs streams of atomized, high-velocity particles toward a substrate, and (c) electron beam melting, which bonds powdered material under a high vacuum layer-by-layer via an electron beam.

Manuscript received October 15, 2018; final manuscript received June 7, 2019; published online June 21, 2019. Assoc. Editor: Y. Kevin Chou.

AM process, as governed by the first law of thermodynamics, by employing relevant input material properties.

Heating of materials by way of laser-based processes is attractive in manufacturing due to the precision that it offers, with a nominal focus diameter not larger than 0.5 mm. Lasers offer a highly controllable method to deliver the necessary amount of localized energy to process powdered material due to its collimated (parallel) and monochromatic energy and to its ability to pulse at a prescribed frequency by beam chopping or by modulating the voltage. Some typical lasers used are yttrium aluminum garnett for processing ceramics and metals and carbon dioxide (CO_2) for polymeric materials. Industrial lasers range in power, approximately from 1 to 10,000 W for polymeric materials. However, if not properly controlled, laser procedures can cause excessive variability in the quality of the as-built parts as well as thermal damage to the material and the substrate. These concerns have motivated the present work, in which we build a lumped mass thermal model based to simulate temperature changes of dry Nylon 6 powder due to input power from a laser beam, based on the SLS process. This model will allow us to quantify the sensitivity of the material temperature based on perturbations of the input laser power. We explore the thermal sensitivity on two lumped mass geometries: a cylindrical and a spherical domain, embedded in a previously solidified substrate.

The outline of the paper is as follows. Initially, we must build a thermal model that allows us to achieve a target temperature *without phase transformations*, by energy balance of a control volume that accounts for

- incoming laser irradiance,
- heat conduction into the substrate,
- forced convection from an exhaust system, and
- infrared radiation to the surroundings.

We then represent this thermal model numerically, with expanded functionality to include phase changes.

An uncertainty quantification is carried out by nondimensional parameters that describe the relative contribution of each thermal term. One key advantage of this framework is that it is amenable to a sensitivity analysis. Accordingly, uncertainty quantification studies are also undertaken to ascertain the effects of laser input perturbations on variations in the material processed state, with the potential correlation to as-built part quality. Examples will be presented to illustrate the thermal behavior of the numerical model. Due to its simplicity, this framework is designed to be computationally implemented in a straightforward fashion so that it can be easily implemented by researchers in the field, in particular those working with AM technologies.

Remark. Specifically, AM is usually defined as the process of free-form deposition of materials to build up structures from 3D computer-aided design (CAD) data, as opposed to material-removal processes such as machining and abrasion (ASTM). Huang et al. [22] provide an overview of research activities in the AM community. We denote that 3D printing (3DP) is synonymous to AM, a term that has typically received the bulk of the attention, mainly from commercial low-end hobbyist printers. This process utilizes solid models built in a CAD package, which are sliced into layers for sequential printing. ■

2 Contributing Thermal Terms

Defining a "building block," we begin by considering a control volume of a lumped mass for a sample of material after it is deposited on a substrate with a prescribed temperature, as shown in Fig. 1. For now, we prescribe *no phase transformations or mass losses* in order to properly estimate the power intensity of the laser that will induce a temperature rise in within a specific time duration, or dwell time, over the sample. This thermal model will serve as the basis for this research. The first law of thermodynamics serves as our governing equation in order to perform an overall balance to quantify the rate of change of the stored energy ($\dot{W}$) and the heat input, which in

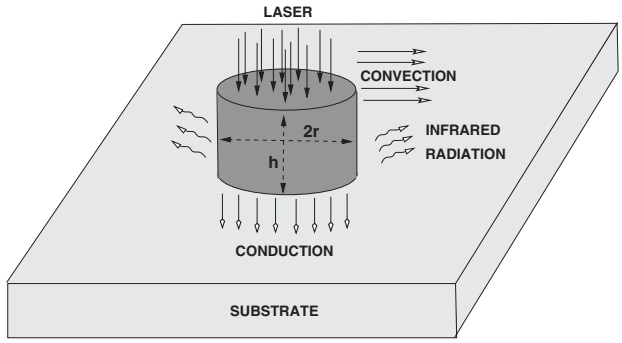

Fig. 1 An idealized powder particle domain deposited on a substrate material and irradiated by laser energy

the simple case of no mass transfer and constant heat capacity reads as $\left(\dot{W} = (d/dt)(MH\theta) = MH\dot{\theta}\right)$

$$MH\dot{\theta} = \mathcal{L}_1 + \mathcal{L}_2 + \mathcal{L}_3 + \mathcal{L}_4 \tag{1}$$

where M is the mass inside of the control volume and H is the thermodynamic heat capacity, which is more detailed in Sec. 5. Both M and H are assumed constant, initially. We have the following contributing effects (denoted $\mathcal{L}_1 \rightarrow \mathcal{L}_4$):

- Absorbed incident optical radiation (laser beam): $\mathcal{L}_1 \stackrel{\text{def}}{=} I^a A_I = (I^i - I^r)A_I$, where I^a is the absorbed radiation per unit area, $I^r = RI^i$ is the reflected radiation, R is the reflectivity of the material, I^i is the incident radiation per unit area, and A_I is the area of the exposed (irradiated) surface.
- Conduction to the substrate (base): $\mathcal{L}_2 \stackrel{\text{def}}{=} (IK/L)(\theta_B - \theta)A_B$, where θ and θ_B are the temperatures of the material and of the substrate (base) onto which the target material is deposited, respectively, A_B is the area of contact between the base and the target material, IK is the thermal conductivity of the material, and L is the length scale across which thermal conduction occurs.
- Emitted thermal radiation: $\mathcal{L}_3 \stackrel{\text{def}}{=} \epsilon\sigma(\theta_S^4 - \theta^4)A_{RS} + \epsilon\sigma(\theta_B^4 - \theta^4)A_{RB}$, where θ_S is the temperature of the surrounding air in the build chamber, $0 \le \epsilon \le 1$ is the target material emissivity, $\sigma = 5.670373 \times 10^{-8}$ (W/m^2 K^4) is the Stefan–Boltzmann constant, A_{RS} is the area of the radiative surface exposed to the surroundings and $A_{RB} = A_B$ is the area of the radiative surface in contact with the substrate material.
- Convection (e.g., from an exhaust system): $\mathcal{L}_4 \stackrel{\text{def}}{=} h_C(\theta_S - \theta)A_C$, where h_C is the effective surface convection coefficient, and A_C is the area of the convective surface exposed to the surroundings.

3 Relative Contributions: Order of Magnitude Analysis

In this section, we create nondimensional parameters for each thermal contribution so that we can ultimately quantify the sensitivity of the model due to each term. We achieve this by normalizing the governing equation (1), yielding

$$\dot{\theta} = \frac{I^a A_I}{MH}\left(1 + \frac{\mathcal{L}_2}{\mathcal{L}_1} + \frac{\mathcal{L}_3}{\mathcal{L}_1} + \frac{\mathcal{L}_4}{\mathcal{L}_1}\right) \tag{2}$$

The nondimensional expressions of the contributing thermal terms are defined according to Fig. 1, leaving behind the pertaining temperatures, the dimensions of the target control volume, and the laser power as variables,

- The ratio of conductive to laser contributions is

$$\frac{Conduction}{Laser} = \frac{\mathcal{L}_2}{\mathcal{L}_1} = \frac{IK(\theta_B - \theta)A_B}{LI^a A_I} \approx \frac{\mathcal{O}(10^{-1})(\theta_B - \theta)A_B}{LI^a A_I} \approx \frac{\theta_B - \theta}{LI^a}\mathcal{O}(10^{-1}) \tag{3}$$

  where $0.1 \leq IK \leq 0.5$ (W/m K) for typical polymeric materials, and the ratio of the areas is assumed to be of order unity ($A_I \approx A_B$).
- The ratio of infrared radiation to laser contributions is

$$\frac{Radiation}{Laser} = \frac{\mathcal{L}_3}{\mathcal{L}_1} = \frac{\epsilon\sigma(\theta_S^4 - \theta^4)A_{RS}}{I^a A_I} + \frac{\epsilon\sigma(\theta_B^4 - \theta^4)A_{RB}}{I^a A_I} \approx \frac{\mathcal{O}(10^{-1})\mathcal{O}(10^{-8})(\theta_S^4 - \theta^4)(A_{RS} + A_{RB})}{I^a A_I} \approx \frac{\theta_S^4 - \theta^4}{I^a}\mathcal{O}(10^{-9}) \tag{4}$$

  where the ratio of the areas is once again assumed to be of order unity ($A_I \approx A_{RB} + A_{RS}$).
- The ratio of convective to laser contributions is

$$\frac{Convection}{Laser} = \frac{\mathcal{L}_4}{\mathcal{L}_1} = \frac{h_C(\theta_S - \theta)A_C}{I^a A_I} \approx \frac{\mathcal{O}(10^{-1})(\theta_S - \theta)A_C}{I^a A_I} \approx \frac{\theta_S - \theta}{I^a}\mathcal{O}(10^{-1}) \tag{5}$$

  again, the ratio of the areas is assumed to be of order unity ($A_I \approx A_C$).

Even though we assume that the polymer material absorbs a smaller portion of the incident irradiance than the reflected irradiance, we can still rewrite the absorbed irradiance per unit area in terms of the power input, $I^a \approx P\beta/A_I$ where $\beta = \mathcal{L}_1/P$ denotes the fraction of absorbed power, yielding

- The ratio of conductive to laser contributions is

$$\frac{Conduction}{Laser} \approx \frac{\theta_B - \theta}{L\dfrac{P\beta}{A_I}}\mathcal{O}(10^{-1}) \tag{6}$$

- The ratio of infrared radiation to laser contributions is

$$\frac{Radiation}{Laser} \approx \frac{\theta_S^4 - \theta^4}{\dfrac{P\beta}{A_I}}\mathcal{O}(10^{-9}) \tag{7}$$

- The ratio of convective to laser contributions is

$$\frac{Convection}{Laser} \approx \frac{\theta_S - \theta}{\dfrac{P\beta}{A_I}}\mathcal{O}(10^{-1}) \tag{8}$$

Using dermatological applications as a guiding standard for the laser power input, we can say that it ranges as $P\beta = 10^n$ W ($0 \leq n \leq 3$). Assuming that we can focus the entire irradiance per unit area on the target, we can express this quantity as

$$\frac{1}{A_I} \leq I^a \leq \frac{10^n}{A_I} \tag{9}$$

and so if we assume $I^a \approx 10^n/A_I$, we can generate the expressions for the dimensionless ratios for each thermal contribution compared with the laser energy with an explicit particle size factor A_I.

- The ratio of conductive to laser contributions is

$$\frac{Conduction}{Laser} \approx \frac{(\theta_B - \theta)A_I}{L}\mathcal{O}(10^{-1-n}) \tag{10}$$

- The ratio of infrared radiation to laser contributions is

$$\frac{Radiation}{Laser} \approx (\theta_S^4 - \theta^4)\ A_I\ \mathcal{O}(10^{-9-n}) \tag{11}$$

- The ratio of convective to laser contributions is

$$\frac{Convection}{Laser} \approx (\theta_S - \theta)\ A_I\ \mathcal{O}(10^{-1-n}) \tag{12}$$

Clearly, for small particle size (or control volume) L, as it is the case in this study, conduction can play a significant role. The idealized protrusion in Fig. 1 serves as an example, with the following geometric quantities:

- Area in contact with base material: $A_B = \pi r^2$,
- Area exposed to the surroundings: $A_C = 2\pi rL + \pi r^2$,
- Area of radiative surface exposed to surroundings: $A_{RS} = 2\pi rL + \pi r^2$,
- Area of radiative surface exposed to base material: $A_{RB} = \pi r^2$ and
- Area exposed to laser energy irradiation: $A_I = \pi r^2$.

For $r \approx L$, this yields $A_I/L \approx L$ and for $r > L$ yields $A_I/L > r$. These relationships hint at the fact that, for a small target measuring $r \approx 10^{-4}$ m, the thermal conduction term will dominate the energy balance, and it could become on the order of the laser input.

Note that these comparative ratios are dynamic due to changing temperature difference factor during material cooling or heating. Most notably, the infrared radiation to laser input ratio expression will undergo the most change since it is a function of temperatures raised to the fourth power. Therefore, we expect that radiation effects will not be significant when the material maintains a low temperature, but it will become a major contributor to the thermal field during higher material temperatures.

4 Analytics: Thermal Responses for Special Cases

In order to obtain insight into the sensitivity of the system response, we now consider special cases that are amenable to analytical methods. Afterward, we will treat the system numerically with phase transformations included.

4.1 Special Thermal Cases

4.1.1 Case 1: Laser Irradiance and Conduction. Consider now a special case of the general set of thermal models where we only consider laser irradiation and conduction. Equation (1) simplifies to

$$MH\dot{\theta} = I^a A_I + \frac{IKA_B}{L}(\theta_B - \theta) \tag{13}$$

and it can be solved analytically, assuming $\theta(t=0) = \theta_B$, yielding

$$\theta(t) = \theta_B + \frac{I^a A_I L}{IKA_B}\left(1 - e^{-\frac{IKA_B t}{MHL}}\right) \tag{14}$$

This relationship allows us to observe that

- The rise time for the temperature is dictated by the ratio of the conduction to the thermodynamic heat capacity IKA_B/MHL.
- At steady-state, $e^{-\frac{IKA_B t}{MHL}} \to 0$ and

$$\theta_\infty = \theta_B + \frac{I^a A_I L}{IKA_B} \tag{15}$$

  which indicates that the ratio of I^a to IK/L dictates the steady-state temperature θ_∞ (assuming $A_I \approx A_B$).

- A substrate design or material that highly promotes thermal conduction, where the conductive losses of the control volume are instantaneous, we have $IK \to \infty$ and $\theta(t) = \theta_B$.
- A substrate design that is highly insulating, where the conductive losses are zero, we have $IK \to 0$ and $\theta(t) = \theta_B + (I^a A_I t / MH)$. Here, the control volume will trap a maximum amount of heat, and the radiative term will be increasingly more important in the energy balance equation.

4.1.2 Case 2: Laser Irradiance, Conduction, and Convection. Convection is an ever-present phenomenon and an integral part of AM processes since it helps to control the cooling profile of the part, both during and after printing. Accordingly, we add convection to Case 1, leading to

$$MH\dot{\theta} = I^a A_I + \frac{IKA_B}{L}(\theta_B - \theta) + h_C A_C(\theta_S - \theta) \tag{16}$$

which yields a known analytical solution of

$$\theta(t) = \left(\theta_B - \frac{B}{A}\right)e^{-At} + \frac{B}{A} \tag{17}$$

where we have

$$A = \left(\frac{IKA_B}{MHL} + \frac{h_C A_C}{MH}\right) \tag{18}$$

and

$$B = \left(\frac{IKA_B\theta_B}{MHL} + \frac{h_C A_C \theta_S}{MH} + \frac{I^a A_I}{MH}\right) \tag{19}$$

The quotient is

$$\frac{B}{A} = \frac{\dfrac{IKA_B\theta_B}{MHL} + \dfrac{h_C A_C \theta_S}{MH} + \dfrac{I^a A_I}{MH}}{\dfrac{IKA_B}{MHL} + \dfrac{h_C A_C}{MH}} = \frac{\dfrac{IKA_B\theta_B}{L} + h_C A_C \theta_S + I^a A_I}{\dfrac{IKA_B}{L} + h_C A_C} \tag{20}$$

Inverting the solution to solve for the time for the temperature to reach a critical temperature, such as a known burning temperature $\theta(t) = \theta^*$, yields

$$t = t^* = \ln\left(\frac{\theta^* - \dfrac{B}{A}}{\theta_B - \dfrac{B}{A}}\right)^{-\frac{1}{A}} \tag{21}$$

Note that when the argument of the logarithmic function is negative, the system can never reach the burning temperature. For the range of parameters in this study, the denominator always remains negative, thus the sign of the numerator dictates whether the laser power is sufficient to reach the burning temperature. Explicitly,

$$\theta^* - \frac{B}{A} \le 0 \Rightarrow \frac{B}{A} = \frac{\dfrac{IKA_B\theta_B}{L} + h_C A_C \theta_S + I^a A_I}{\dfrac{IKA_B}{L} + h_C A_C} \ge \theta^* \tag{22}$$

Very strong conduction and/or convection at the laser intensity setting chosen can cause an inability to meet this criterion. According to Eq. (21), as the convective coefficient approaches infinity $h_C \to \infty$, the time to burning also increase to infinity $t^* \to \infty$. Furthermore, from Eq. (20), as the convective coefficient increases to infinity $h_C \to \infty$, then $B/A \to \theta_S$. In this case, a specified critical temperature θ^* can never be reached.

4.2 Sensitivity Analyses. An important question to address is the sensitivity of the thermal response to the system parameters. In this study, we pay special attention to laser power input perturbations. Since we assume that the power delivery rate is uniform for a desired simulated dwell time $\tilde{t}$, then the laser must be stationary above the domain. In the case of a laser in motion, the power delivery rate during $\tilde{t}$ would be variable according to a Gaussian shape of a typical laser beam. Specifically, consider the cases in the following sections.

4.2.1 Case 1: Laser Irradiance and Conduction.

- Sensitivity to laser energy input

  We find the sensitivity of the temperature of the material to the laser power input perturbations ∂I^a with Eq. (14) such that

$$\frac{\partial\theta(t)}{\partial I^a} = \frac{A_I L}{IKA_B}\left(1 - e^{-\frac{IKA_B t}{MHL}}\right) \tag{23}$$

  As $t \to \infty$,

$$\frac{\partial\theta(t)}{\partial I^a} \to \frac{A_I L}{IKA_B} = \frac{A_I}{A_B}\frac{L}{IK} \tag{24}$$

  which clearly shows the sensitivity's dependence on the dimensionless ratio of the area of the laser and the area on the conductive base.
- Process variation

  A variation of the laser power ΔI^a is one parameter that can cause process variation $\Delta\theta$. This variation could arise from extrinsic factors such as human error, gradual fouling of the laser lens, fluctuations of power in the laboratory, etc. To understand this effect, we consider ΔI^a as the sole source of process variation. We express this as

$$\Delta\theta = \frac{\partial\theta(t)}{\partial I^a}\Delta I^a = \underbrace{\left(\frac{A_I L}{IKA_B}\left(1 - e^{-\frac{IKA_B t}{MHL}}\right)\right)}_{\alpha(t)}\Delta I^a \tag{25}$$

  As $t \to \infty$,

$$\Delta\theta = \frac{\partial\theta(t)}{\partial I^a}\Delta I_a = \underbrace{\left(\frac{A_I}{A_B}\frac{L}{IK}\right)}_{\alpha^\infty}\Delta I^a \tag{26}$$

Predefining a laser dwell time over the material $\tilde{t}$, we can define the process variation as

$$\Delta\theta(\tilde{t}) = \frac{\partial\theta(\tilde{t})}{\partial I^a}\Delta I^a = \underbrace{\left(\frac{A_I L}{IKA_B}\left(1 - e^{-\frac{IKA_B \tilde{t}}{MHL}}\right)\right)}_{\alpha(\tilde{t})}\Delta I^a \tag{27}$$

Explicitly, $\Delta\theta(\tilde{t})$ represents the range of temperatures expected, across all samples, at the end of the dwell time $\tilde{t}$ if we expect the laser intensity to vary within the predetermined perturbation range ΔI^a. Assuming that the laser intensity parameter variation has a uniform distribution, a standard deviation of the variation response $\theta(\tilde{t})$ can be quantified.

4.2.2 Case 2: Laser Irradiance, Conduction, and Convection.

- Sensitivity to laser energy input

  We find the sensitivity of the final temperature of the material due to laser power input perturbations ∂I^a using Eq. (17) such that,

$$\frac{\partial\theta(t)}{\partial I^a} = \frac{A_I(1 - e^{-At})}{\dfrac{IKA_B}{L} + h_C A_C} \tag{28}$$

As $t \to \infty$,

$$\frac{\partial \theta(t)}{\partial I^a} \to \frac{A_I}{\frac{IKA_B}{L} + h_C A_C} \tag{29}$$

which clearly shows the sensitivity's dependence on the dimensionless ratio of the area of the laser, the area on the conductive base, and the convective area.

- Process variation

Again, we consider the process variation due to predetermined perturbations of laser intensity from extrinsic factors such that

$$\Delta\theta = \frac{\partial \theta(t)}{\partial I^a}\Delta I_a = \underbrace{\left(\frac{A_I(1-e^{-At})}{\frac{IKA_B}{L} + h_C A_C}\right)}_{\alpha(t)}\Delta I_a \tag{30}$$

As $t \to \infty$,

$$\Delta\theta = \frac{\partial \theta(t)}{\partial I^a}\Delta I_a \to \underbrace{\left(\frac{A_I}{\frac{IKA_B}{L} + h_C A_C}\right)}_{\alpha^\infty}\Delta I_a \tag{31}$$

which clearly shows the sensitivity's dependence on the dimensionless ratio of the area of the laser, the area on the conductive base, and the convective area.

Finally, we define the process variation for a certain laser irradiation dwell time,

$$\Delta\theta(\tilde{t}) = \frac{\partial \theta(\tilde{t})}{\partial I^a}\Delta I_a = \underbrace{\left(\frac{A_I(1-e^{-A\tilde{t}})}{\frac{IKA_B}{L} + h_C A_C}\right)}_{\alpha(\tilde{t})}\Delta I_a \tag{32}$$

In all cases, the factor α is the multiplier which indicates the scaling of the laser input perturbation. In all cases, high conductivity and high convection lead to less sensitivity due to laser perturbations.

5 General Time-Transient Simulations With Phase Transformations

Until this point in the analysis, we have not included phase transformations and latent heats. At this point, we must be more careful with the definition of heat capacity. For example, consider a widely used model, writing the thermodynamic stored energy rate directly as

$$\frac{dW}{dt} = \frac{d(Mw)}{dt} = \frac{dM}{dt}w + M\frac{dw}{dt} = \frac{dM}{dt}w + M\frac{\partial w}{\partial \theta}\frac{d\theta}{dt} = \frac{dM}{dt}w + MH\frac{d\theta}{dt} \tag{33}$$

Here, w is the energy per unit mass and $H = \partial w/\partial\theta$ represents the thermodynamic specific heat capacity. Thus,

$$\dot{W} = \dot{M}w + MH\dot{\theta} = \mathcal{L}_1 + \mathcal{L}_2 + \mathcal{L}_3 + \mathcal{L}_4 \tag{34}$$

Remark. An alternative simple model, used often in continuum mechanics applications, is to write the thermodynamic stored energy directly as

$$W = MC\theta \tag{35}$$

which is rather phenomenological. The heat capacity parameter C is time-dependent (implicitly through θ dependency). The rate of energy reads as

$$\frac{dW}{dt} = \dot{M}C\theta + M\dot{C}\theta + MC\dot{\theta} \tag{36}$$

thus

$$\dot{W} = \frac{d}{dt}(MC\theta) = \dot{M}C\theta + M\dot{C}\theta + MC\dot{\theta} = \mathcal{L}_1 + \mathcal{L}_2 + \mathcal{L}_3 + \mathcal{L}_4 \tag{37}$$

Equations (34) and (37) are mathematically equivalent. To see this, one can write

$$\dot{W} = \dot{M}w + MH\dot{\theta} = \dot{M}C\theta + M\dot{C}\theta + MC\dot{\theta} \tag{38}$$

For example, in the case where $\dot{M} = 0$

$$\dot{W} = MH\dot{\theta} = M\dot{C}\theta + MC\dot{\theta} \Rightarrow H\dot{\theta} = \dot{C}\theta + C\dot{\theta} \tag{39}$$

or, alternatively

$$\frac{\partial w}{\partial \theta} = H = \frac{\partial C}{\partial \theta}\theta + C \tag{40}$$

The advantages of one representation over another depend on the data available. Despite some mathematical advantages in using the model in Eq. (35) (in cases of mass transfer), we will continue to use the model in Eq. (34), due to the more readily available data. ■

5.1 Phase Transformations. To include phase transformations, for example, melting and solidification, we include a thermally dependent heat capacity (due to latent heats, and the material phase) by utilizing the following cases:

- *Solid → solid*: If $\theta(t) < \theta_m$ and $\theta(t+\Delta t) < \theta_m$ then no melting occurs, so we use $H(\theta(t)) = H_S$ in the governing equation.
- *Solid → liquid*: If $\theta(t) < \theta_m$ and $\theta(t+\Delta t) \geq \theta_m$ then melting occurs, so we use $H(\theta(t)) = H_S + (\delta\mathcal{P}^{S\to L}/\delta\theta)$ in the governing equation.
- *Liquid → liquid*: If $\theta(t) \geq \theta_m$ and $\theta(t+\Delta t) \geq \theta_m$ then material remains melted, so we use $H(\theta(t)) = H_L$ in the governing equation.
- *Liquid → solid*: If $\theta(t) \geq \theta_m$ and $\theta(t+\Delta t) < \theta_m$ then solidification occurs, so we use $H(\theta) = H_L + (\delta\mathcal{P}^{L\to S}/\delta\theta)$ in the governing equation.

Here, H_S is the solid phase heat capacity and H_L is the liquid phase heat capacity and

- $0 < \delta\mathcal{P}^{S\to L}$ represents the latent heat of melting,
- $0 < \delta\mathcal{P}^{L\to S}$ represents the latent heat of solidification, and
- $0 < \delta\theta$ represents a "bandwidth" over which the phase transformation takes place.

Remark 1. Latent heats are defined to represent the energy absorbed or released to transform the material from one initial phase to the new phase during a *constant-temperature* process for a certain time interval. In this case, we want to observe the effects of a *constant energy input rate* on the material temperature. ■

The latent heats modify the heat capacity term H inside of the temperature bandwidth $\delta\theta$ so that physically correct effects of a phase change are captured. For example, in the case of melting (solid to liquid), the latent heat of melting increases the heat capacity during the phase transformation and so a low-temperature rise can be observed.[2] This model is relatively straightforward to include within the upcoming computational framework.

Remark 2. We can also include a material burn off represented as vaporization, which is discussed in Sec. 8. This process can also involve mass transfer out of the control volume, thus $\dot{M} \neq 0$. ■

5.2 System Discretization. We employ an implicit trapezoidal rule time integration scheme for solving the balance of energy (assuming that the mass is constant). This time integration

[2]In the idealized limit, the temperature would be constant.

scheme calculates the material temperature at a half time step ($\phi = 0.5$) with contributions from the temperatures at the current time step and at the next time step. We first guess the temperature at the next time step and then we iterate until we converge on a solution, within a prescribed tolerance. Normally, we were able to gain convergence well within six iterations. In this study, we chose $\phi = 0.5$, meaning that the contributions from the temperatures at the current and at the next time step have equal weights. Again, the governing equation for energy balance is

$$MH\dot{\theta} = \mathcal{L}_1 + \mathcal{L}_2 + \mathcal{L}_3 + \mathcal{L}_4 \tag{41}$$

thus,

$$\dot{\theta}|_{t+\phi\Delta t} \approx \frac{\theta(t+\Delta t) - \theta(t)}{\Delta t} = \frac{1}{MH(t+\phi\Delta t)}\left((\mathcal{L}_1 + \mathcal{L}_2 + \mathcal{L}_3 + \mathcal{L}_4)|_{t+\phi\Delta t}\right)$$

leading to

$$\theta(t+\Delta t) = \theta(t) + \left(\frac{\Delta t}{MH}\mathcal{L}_1 + \mathcal{L}_2 + \mathcal{L}_3 + \mathcal{L}_4\right)|_{t+\phi\Delta t} \tag{42}$$

The solution procedure is straightforward. At a given time step:

- *Step 1:* Update temperature

$$\theta^{k+1}(t+\Delta t) = \theta(t) + \left(\frac{\Delta t}{MH}(\mathcal{L}_1 + \mathcal{L}_2 + \mathcal{L}_3 + \mathcal{L}_4)\right)^k|_{t+\phi\Delta t} \tag{43}$$

- *Step 2:* Check for phase transformations and update $H(t+\phi\Delta t)$.
- *Step 3:* Iterate until convergence ($k = 1,\ldots.$) to within a predetermined tolerance, and time is advanced.
- *Step 4:* Repeat steps 1–3 at the next time step.

6 Numerical Examples With Laser Perturbations

We consider the idealized lumped mass cylindrical domain shown in Fig. 1, irradiated by a prescribed laser power P in Watts. The parameters used pertained to material properties of a typical polyamide Nylon 6, which is widely used in SLS processes.

6.1 Lumped Mass Problem Definition. The material properties and process parameters were as follows:

- $L = 80.1\ \mu$m,
- $r = 80.1\ \mu$m,
- $\theta_B = 295$ K,
- $\theta_S = 295$ K,
- $\theta^* = 10^6$ K,
- $\rho = 1130$ kg/m^3,
- $IK = 0.23$ W/m K,
- $\epsilon = 0.75$, and
- $h_C = 5.7$ W/m^2 K,

where the particle size geometries L and r are based on a mean particle size of a proprietary dry Nylon 6 powder formulation commercialized by BASF for SLS processing; the temperature parameters θ_B, θ_S, and θ^* were based on real process settings typically employed by researchers at BASF laboratories; the thermal conductivity ϵ value follows work from experimental methods by Okada et al. [23]; the density ρ and conductivity IK values taken from data published by the Polymer Data Handbook [24]; and the convection coefficient assumes free convection values based on Eq. (1) as reported by Sartori [25] for a vertical plate.

A population of these idealized lumped mass domains were subjected to laser power perturbations. Generated P_i parameter input values, where $i = 1, 2, \ldots N$, were based on an evenly spaced uniform distribution with a range of $\pm\Delta P$ and mean $\bar{P}$ to simulate perturbations in the laser power input from extrinsic effects (again, human error or lens fouling). Furthermore, a battery of cases at various $\bar{P}$ levels were run, each corresponding to a laser power intensity level I^a, in order to quantify its effects on the sensitivity of the thermal field at time $\tilde{t}$. For these stochastic studies, we used the following laser input and sample population parameters:

- $N = 100$ samples,
- $0.004\ \text{W/m}^2 \le I^a \le 1.5\ \text{W/m}^2$,
- $\Delta P/\bar{P} = 0.1$,
- $\tilde{t} = 1$ s,

For the possible phase transformations, we used Nylon 6 thermodynamic data reported by studies performed by Millot et al. [26] and data published by the *Polymer Data Handbook* [24]. These parameters are as follows:

- $\theta_m = 493$ K,
- $H_S(\theta) = 4.502 \cdot \theta + 138.7$ J/kg K,
- $H_L(\theta) = 1.348 \cdot \theta + 1979.3$ J/kg K,
- $\delta\mathcal{P}^{S\to L}/\delta\theta = 1$ J/kg K,
- $\delta\mathcal{P}^{L\to S}/\delta\theta = 1$ J/kg K.

Also, we assumed that the surrounding substrate and environment are heat sinks whose temperatures are constant. The time-step size Δt was chosen to be sufficiently small so that the results are not sensitive to further reductions of Δt. This indicates that we expect the results to contain a negligible numerical error.

6.2 Uncertainty Quantification. This section gives a brief overview of the moments of distributions for developing uncertainty calculations. Any generic quantity of interest Y with a distribution of values $Y = \{Y_1, Y_2, \ldots, Y_N\}$ has moments about an arbitrary reference point, denoted $Y^\star$, as follows:

$$\mathbf{Z}_r^{Y_i - Y^\star} \overset{\text{def}}{=} \frac{\sum_{i=1}^{N_p} a_i (Y_i - Y^\star)^r}{\sum_{i=1}^{N_p} a_i} \overset{\text{def}}{=} \overline{(Y_i - Y^\star)^r} \tag{44}$$

where r denotes the "rth" moment of the distribution. The various moments characterize the distribution, for example:

(1) $\mathbf{Z}_1^{Y_i-\mu}$ equals zero as it measures the first deviation about the mean μ,
(2) $\mathbf{Z}_1^{Y_i-0} \overset{\text{def}}{=} \sum_{i=1}^{N_p} a_i(Y_i - 0)/\sum_{i=1}^{N_p} a_i \overset{\text{def}}{=} \overline{(Y_i - 0)} = \mu$, is the mean
(3) $\mathbf{Z}_2^{Y_i-\mu}$ is the standard deviation,
(4) $\mathbf{Z}_3^{Y_i-\mu}$ is the skewness (third moment), which is an indicator of the asymmetry, or bias, and
(5) $\mathbf{Z}_4^{Y_i-\mu}$ is the kurtosis (fourth moment), which indicates the "tightness" of the distribution.

The two most important quantities are the mean (μ) and the standard deviation (S), and a key dimensionless quantity is S/μ which can be interpreted either as the quantification of the uncertainty around the mean or as a percentage error. For the purposes of this analysis, $a_i = 1$, $\mu = \bar{\theta}(\tilde{t})$, and $S = \Delta\theta(\tilde{t})$. We must quantify $\Delta\theta/\bar{\theta}$ at each laser power intensity level I^a based on the distribution of the final material temperatures $\theta(\tilde{t})$ across the N samples. This $\Delta\theta/\bar{\theta}$ quantification serves as a gauge for the process sensitivity; a higher value corresponds to a wider spread of final temperatures.

6.3 Numerical Results. Figures 2(*a*) and 2(*b*) depict the process sensitivity results varying the input wattage between $0.004 - 1.5$ W. These plots show the normalized standard deviation $\Delta\theta/\bar{\theta}$, otherwise known as the sensitivity, of the final temperatures from five cases:

(1) Isolated thermal contributions from conduction,
(2) Isolated thermal contributions from convection,
(3) Isolated thermal contributions from radiation,
(4) No cooling, and
(5) All thermal contributions (conduction, convection, and radiation).

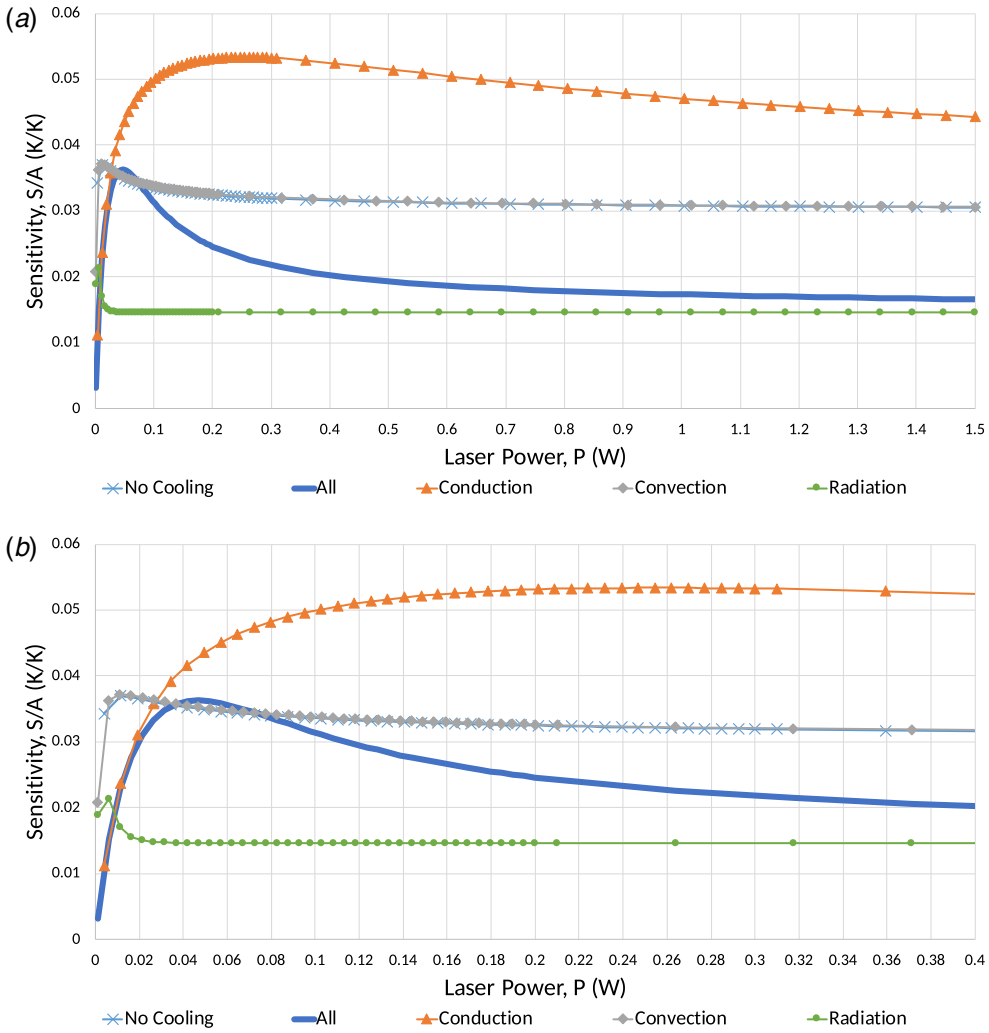

Fig. 2 Cylindrical domain: sensitivity of final temperatures due to laser irradiation perturbations for a lumped mass for cases (1) without thermal contributions (no cooling), (2) with all thermal contributions, and (3)–(5) with isolated thermal contributions: (*a*) sensitivity of final temperatures due to laser irradiation perturbations and (*b*) a more detailed view of the high-sensitivity area

Table 1 illustrates the average resulting temperature $\bar{\theta}$, the standard deviation $\Delta\theta$, and the normalized standard deviation, or sensitivity, with perturbations of the laser input power. The peak normalized standard deviation occurs at approximately 0.05 W, and so material samples will experience an irradiation within the range of 0.05 W ±10%. Material samples experiencing laser irradiation closer to the higher bound will have fully attained their steady-state temperature, whereas the samples that experience laser inputs closer to the lower bound are in the process of heating up toward their steady-state temperature. As expected, the steady-state temperature is unique for each laser power input level, and it is based on the cooling effects from radiated heat at higher material temperatures.

Table 1 Cylindrical domain: thermal variation as a function of laser input power with perturbations. The peak normalized standard deviation occurs when some sample have reached their steady-state temperature and others have not, at approximately 0.05 W.

$\bar{P}$, Avg. Input (W)	$\bar{\theta}$, Avg. Final Temp. (K)	$\Delta\theta$, Std. Deviation (K)	$\frac{\Delta\theta}{\bar{\theta}}$
0.001	312.06	1.00	0.0032028
0.04	962.74	34.77	0.036123
0.08	1451.62	48.35	0.033308
0.12	1797.73	52.48	0.029197
0.16	2028.36	54.05	0.026650

Samples that have reached the steady-state temperature have transitioned from chiefly conductive cooling to radiative cooling. As the laser input power continues to be increased, more and more material samples will have reached their steady-state temperature and so the range of the final temperatures gets increasingly tighter. To reinforce these conjectures, we must focus on the trends on Figs. 2(*a*) and 2(*b*), especially on the bold line that represents the process sensitivity for the case when all thermal contributions are considered. Initially, between 0.004 and 0.04 W, this bold line closely follows the trend when *only conduction* is considered, serving as evidence that the effects due to conduction indeed dominate the thermal balance within this laser power input range. However, with higher laser power, the material is allowed to reach higher final temperatures, and radiation takes over as this term is a function of temperature raised to the fourth power. The bold line now deviates from the conduction-only case and approaches the radiation-only trend. Ultimately, the effects due to radiation will overcome the effects by conduction and convection.

It is interesting to note that for the surface convection coefficient h_C chosen, its effects are negligible. We can make this claim since the sensitivity trend for the case with just convection follows closely

the trend for the case without cooling effects. In this study, the surface convection coefficient was set at $h_C = 5.7$ W/m^2 K, yielding sensitivity differences between these cooling cases within 1.3×10^{-5}. We must also make note that these results chiefly pertain to the material of choice: Nylon 6.

The temperatures are, of course, unrealistically high after melting (and would probably vaporize) and are just for illustration purposes. In these cases, one should consider vaporization and mass transfer, which is discussed in Sec. 8.

7 A Modification for a Typical Powder Particle Geometry

A particular example of interest in additive manufacturing is a particle embedded in a powder bed as shown in Fig. 3, which is being irradiated in order to sinter it to the system. This is, of course, the basis of additive manufacturing. The previous algorithm is the same, except that the volume and surface areas are different than the cylindrical domain example discussed previously. We can now define the surface areas in this model problem that affect the energy balance terms.

- Area in contact with base material: $A_B = \frac{1}{2} \times 4\pi r^2$,
- Area exposed to the surroundings: $A_C = \frac{1}{2} \times 4\pi r^2$,
- Area of radiative surface exposed to surroundings: $A_{RS} = \frac{1}{2} \times 4\pi r^2$,
- Area of radiative surface exposed to base material: $A_{RB} = \frac{1}{2} \times 4\pi r^2$ and
- Effectively projected area exposed to laser energy irradiation: $A_I = \pi r^2$.

This yields $A_I/r \approx \pi r$. As an example, assuming a relatively small target with a radius of $r \approx 10^{-3}$ m, the conductive term will be highly significant, as compared with the convective and radiative terms in the energy balance. Additionally, the conductive term could be on the order of the laser input. Thus, fundamentally, the results should be similar to the case with the cylindrical domain with a qualitative shift of the exact power input setting that corresponds to the maximum sensitivity value. In fact, as seen in Fig. 4 and Table 2, the maximum sensitivity has shifted to approximately 0.11 W. This is primarily because of the slight difference of geometric terms that control the relative contributions of convection, conduction, and thermal radiation. Following the same analysis done for a cylindrical domain in Eq. (10), we can quantify the order of magnitudes of the energy balance terms for a sphere.

- The ratio of conductive to laser contributions is

$$\frac{Conduction}{Laser} \approx (\theta_B - \theta)\pi r \ \mathcal{O}(10^{-1-n}) \tag{45}$$

- The ratio of infrared radiation to laser contributions is

$$\frac{Radiation}{Laser} \approx (\theta_S^4 - \theta^4)\pi r^2 \ \mathcal{O}(10^{-9-n}) \tag{46}$$

- The ratio of convective to laser contributions is:

$$\frac{Convection}{Laser} \approx \mathcal{O}(10^{-1-n})(\theta_S - \theta)\pi r^2 \ \mathcal{O}(10^{-1-n}) \tag{47}$$

Fundamentally, the trends are the same. However, these two cases deviate when we consider ablation in Sec. 8.

8 Extensions: General Simulations of Time-Transient Effects With Phase Transformations and Mass Transfer

In some cases, one could also consider vaporization of the material. The governing equation now yields

$$\dot{M}w + MH\dot{\theta} = \mathcal{L}_1 + \mathcal{L}_2 + \mathcal{L}_3 + \mathcal{L}_4 \tag{48}$$

Equation (48) requires that the energy per unit mass be identified. Additionally, we modify the previous solid–liquid cases to yield the following seven cases:

- *Solid → solid*: If $\theta(t) < \theta_m$ and $\theta(t + \Delta t) < \theta_m$ then the material remains a solid, so we use $H(\theta(t)) = H_S$ in the governing equation.
- *Solid → liquid*: If $\theta(t) < \theta_m$ and $\theta(t + \Delta t) \geq \theta_m$ then melting occurs, so we use $H(\theta(t)) = H_S + (\delta \mathcal{P}^{S \to L}/\delta\theta)$ in the governing equation.
- *Liquid → liquid*: If $\theta(t) \geq \theta_m$ and $\theta(t + \Delta t) \geq \theta_m$ then the material remains melted, so we use $H(\theta(t)) = H_L$ in the governing equation.
- *Liquid → solid*: If $\theta(t) \geq \theta_m$ and $\theta(t + \Delta t) < \theta_m$ then solidification occurs, so we use $H(\theta) = H_L + (\delta \mathcal{P}^{L \to S}/\delta\theta)$ in the governing equation.
- *Liquid → vapor*: If $\theta(t) < \theta_v$ and $\theta(t + \Delta t) \geq \theta_v$ then vaporization occurs, so we use $H(\theta(t)) = H_L + (\delta \mathcal{P}^{L \to V}/\delta\theta)$ in the governing equation.
- *Vapor → vapor*: If $\theta(t) \geq \theta_v$ and $\theta(t + \Delta t) \geq \theta_v$ then the material remains a vapor, so we use $H(\theta(t)) = H_V$ in the governing equation.
- *Vapor → liquid*: If $\theta(t) \geq \theta_v$ and $\theta(t + \Delta t) < \theta_v$ then condensation occurs, so we use $H(\theta(t)) = H_V + (\delta \mathcal{P}^{V \to L}/\delta\theta)$ in the governing equation.

As in Sec. 5.1, H_S is the solid phase heat capacity, H_L is the liquid phase heat capacity, and H_V is the thermodynamic heat capacity of the polymer in the gaseous phase and

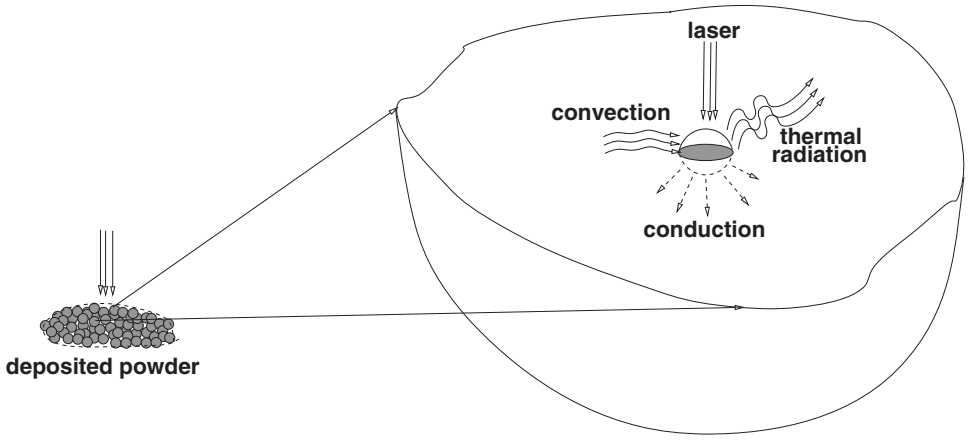

Fig. 3 An idealization of an embedded particle in a powder pack

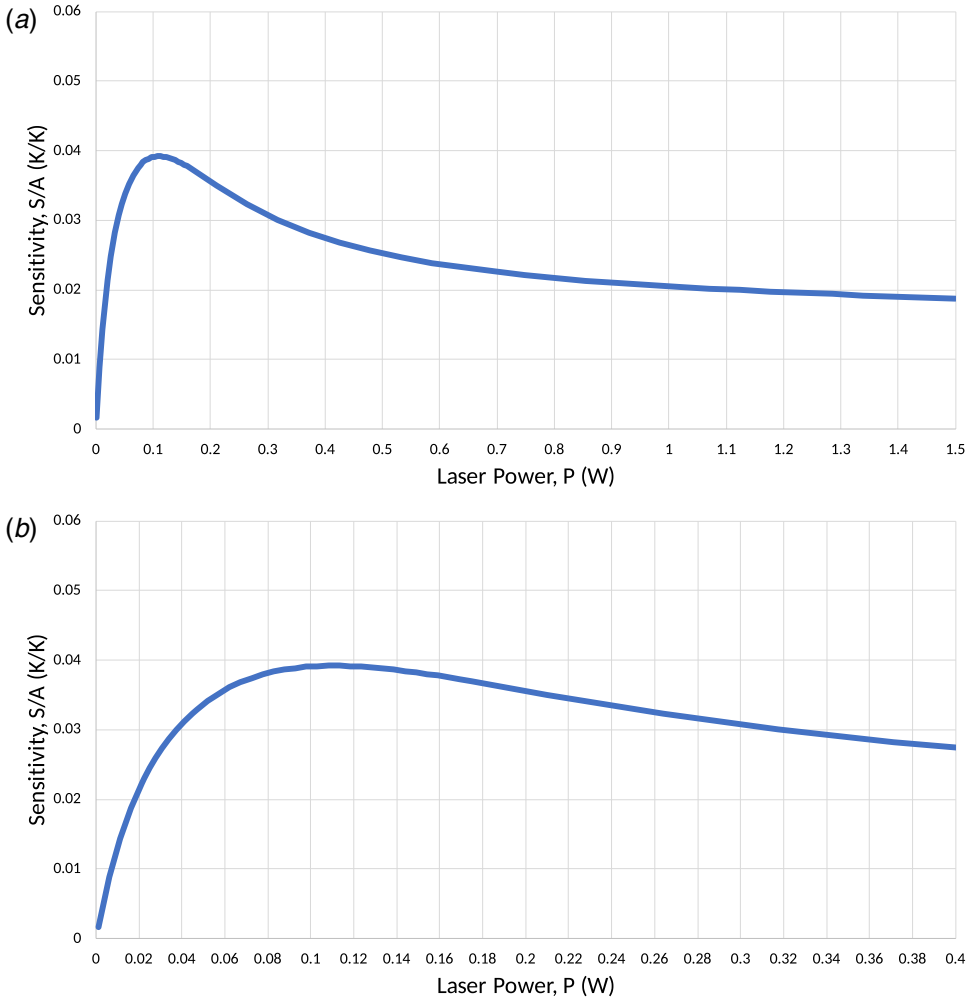

Fig. 4 Spherical domain: sensitivity of final temperatures due to laser irradiation perturbations for a lumped mass with all thermal contributions: (*a*) sensitivity of final temperatures due to laser irradiation perturbations and (*b*) a more detailed view of the high-sensitivity area

Table 2 Spherical domain: thermal variation as a function of laser input power with perturbations. The peak normalized standard deviation occurs when some samples have reached their steady-state temperature and others have not at approximately 0.11 W.

$\bar{P}$, Avg. Input (W)	$\bar{\theta}$, Avg. Final Temp. (K)	$\Delta\theta$, Std. Deviation (K)	$\frac{\Delta\theta}{\bar{\theta}}$
0.001	303.59	0.50	0.001658
0.04	650.46	20.46	0.031462
0.08	980.20	37.56	0.038326
0.12	1279.68	49.98	0.039059
0.16	1511.87	57.08	0.037760

- $0 < \delta\mathcal{P}^{S\to L}$ is the latent heat of melting,
- $0 < \delta\mathcal{P}^{L\to S}$ is the latent heat of solidification,
- $0 < \delta\mathcal{P}^{L\to V}$ is the latent heat of vaporization,
- $0 < \delta\mathcal{P}^{V\to L}$ is the latent heat of condensation, and
- $0 < \delta\theta$ again represents a "bandwidth" over which the phase transformation takes place.

In the case of vaporization, the mass of the target material will be reduced. In order to simulate the time-transient to general melting and *ablation* processes, we must reinforce Eq. (1) to take into account a varying mass rate $\dot{M}$ due to burn-off, evaporation, or even polymeric damage, if tracking mass by molecular weight is preferred. One approach that describes the outflow of mass from the control volume is an evolution law for mass loss that is governed by the thermal field. This relationship is described as

$$\dot{M} = -\zeta M\left(\frac{\theta}{\theta^*} - 1\right) \tag{49}$$

Here, θ^* is the burning temperature, M is the total mass in the control volume, ζ is the rate of removal per unit mass, with the following conditions:

- for above the burning threshold $\theta(t) > \theta^*$: $\zeta = \zeta^* > 0$ and $\dot{M} < 0$, and
- for below the burning threshold $\theta(t) \le \theta^*$: $\zeta = 0$ and $\dot{M} = 0$.

The quantity $(\theta/\theta^* - 1)$ functions as a normalized temperature cut-off function. In this framework, we can assume that the critical burn-off temperature is equivalent to the vaporization temperature θ_V.

8.1 System Discretization. As before, we employ an implicit Trapezoidal Rule time discretization ($\phi = 0.5$) for the energy balance in Eq. (48), yielding

$$\dot{\theta}|_{t+\phi\Delta t} \approx \frac{\theta(t+\Delta t) - \theta(t)}{\Delta t} = \left(\frac{1}{MH}\left(\mathcal{L}_1 + \mathcal{L}_2 + \mathcal{L}_3 + \mathcal{L}_4 - \dot{M}w\right)\right)|_{t+\phi\Delta t} \tag{50}$$

where we can integrate for the temperature at the next time step as

$$\theta(t+\Delta t)=\theta(t)+\left(\frac{\Delta t}{MH}\left(\mathcal{L}_1+\mathcal{L}_2+\mathcal{L}_3+\mathcal{L}_4-\dot{M}w\right)\right)|_{t+\phi\Delta t} \quad (51)$$

In a similar fashion, we can integrate for the vaporized mass loss by employing Eq. (49) as

$$\dot{M}\approx\frac{M(t+\Delta t)-M(t)}{\Delta t}=-\zeta M(t+\phi\Delta t)\left(\frac{\theta(t+\phi\Delta t)}{\theta^*}-1\right) \quad (52)$$

which leads to

$$M(t+\Delta t)=M(t)-\Delta t\zeta M(t+\phi\Delta t)\left(\frac{\theta(t+\phi\Delta t)}{\theta^*}-1\right) \quad (53)$$

We can now build a straightforward procedure to build the solution, as outlined below.

- *Step 1:* Update the temperature at the current iteration step, k:

$$\theta^{k+1}(t+\Delta t)=\theta(t)+\left(\frac{\Delta t}{MH}\left(\mathcal{L}_1+\mathcal{L}_2+\mathcal{L}_3+\mathcal{L}_4-\dot{M}w\right)\right)^k \quad (54)$$

- *Step 2:* Update the mass, also at the current iteration step:

$$M^{k+1}(t+\Delta t)=M(t)-\Delta t\ \zeta\ M^k(t+\phi\Delta t)\left(\frac{\theta^{k+1}(t+\phi\Delta t)}{\theta^*}-1\right) \quad (55)$$

- *Step 3:* Check material temperature to identify phase transformations to update the thermodynamic heat capacity $H(t+\phi\Delta t)$ accordingly. If one assumes that the temperature is constant during phase transformations, then $\dot{H}=0$. However, as noted before, $H(\theta)$ can change independently of a phase transformation, thus $\dot{H}\neq 0$ in those cases.
- *Step 4:* Continue iterations ($k=1, 2, \ldots$) until convergence, and
- *Step 5:* Advance time to the next time step and repeat steps 1–4.

If one were to repeat the preceding simulations for the cylindrical domain, the length of the height L would decrease since the mass would be ablated away. To quantify this change, we can compute the following, noting that in this example r remains constant:

$$M(t)=\rho\pi r^2L(t)\quad\Rightarrow\quad L(t)=\frac{M(t)}{\rho\pi r^2} \quad (56)$$

This relationship shows that as $L\to 0$, radiation plays a much more dominant role at lower laser input power levels (as seen in Fig. 2), while for the spherical domain, assuming a self-similar shrinkage, we have

$$M(t)=\rho\pi\frac{4}{3}r(t)^3\quad\Rightarrow\quad r(t)=\left(\frac{M(t)}{\rho\pi\frac{4}{3}}\right)^{\frac{1}{3}} \quad (57)$$

Here, as $r\to 0$, radiation plays a major role at higher laser input power levels (as seen in Fig. 4), compared with the cylindrical domain.

9 Conclusions and Further Work

While there is certainly a great utility of models for design purposes and for ascertaining trends, there is, however, a limit. To reliably extend this work, more detailed optical and thermal modeling (see, for example, Zohdi [27] and Gross [28] for overviews) should be pursued if it is desirable to understand the laser ray scattering properties of the lumped mass. Techniques that involve functionalized dyes benefit laser-based processes greatly as their enhanced properties can increase the thermal absorption into the material. Electric currents (electrophoresis) direct the application of the dyes in order to precisely target the deposition and interactions, allowing for the operator or researcher to tailor the process for each unique application.

Additionally, the material model can be further refined in order to calculate physical and thermodynamic properties with high fidelity. Using a differential scanning calorimetry curve derived from experimental data for the material at hand and coupled with a thermodynamic model that stochastically calculates the crystalline structure of the solid, this model would integrate the material properties based on the local temperature. This method would allow for the accurate definition of the relationship between the thermodynamic specific heat capacity and the material temperature.

Most critically, the spatial time step sizes for discretization of the thermal fields in a one-, two-, or three-dimensional domain are of interest and require the use of techniques based on, for example, the combinations of finite difference, finite element, and discrete element methods. Furthermore, an aspect of key interest is the characterization of the movement of the domain and potentially hazardous particulate ejecta. Ganeriwala and Zohdi [29], and Zohdi [27,30–32] present a numerical simulation and a comprehensive model of detailed, computationally intensive, modeling of the dynamics and thermodynamics of these phenomena. There are many physical mechanisms that conduce to the creation of ejecta. Electronically induced molecular and macromolecular vibrations are caused by photochemical and electronic ablation, hydrodynamical ablation pertains to the flowing of molten micrometer droplets, and laser energy liberates atomic bonds in photothermal ablation. An example of a purely mechanical process can include exfoliation in which material is removed in flakes by erosion. These mechanisms are not mutually exclusive.

Acknowledgment

The authors acknowledge the generous support of BASF and scientific program managers Andreas Daiss, Wolfgang Gerlinger, and Klaus Stoll.

References

[1] Householder, R., 1979, "Molding Process," U.S. Patent No. 4,247,508.
[2] Deckard, C., 1986, "Method and Apparatus for Producing Parts by Selective Sintering," U.S. Patent No. 4,863,538.
[3] Smith, J., Xiong, W., Yan, W., Lin, S., Cheng, P., Kafka, O. L., Wagner, G. J., Cao, J., and Liu, W. K., 2016, "Linking Process, Structure, Property, and Performance for Metal-Based Additive Manufacturing: Computational Approaches With Experimental Support," Comput. Mech., **57**(4), pp. 583–610.
[4] Voisin, T., Calta, N. P., Khairallah, S. A., Forien, J. B., Balogh, L., Cunningham, R. W., Rollett, A. D., and Wang, Y. M., 2018, "Defects-Dictated Tensile Properties of Selective Laser Melted Ti-6al-4v," Mater. Des., **158**(1), pp. 113–126.
[5] Wang, Z., Yan, W., Liu, W. K., and Liu, M., 2019, "Powder-Scale Multiphysics Modeling of Multi-Layer Multi-Track Selective Laser Melting With Sharp Interface Capturing Method," Comput. Mech., **63**(4), pp. 649–661.
[6] Zohdi, T. I., 2014, "Additive Particle Deposition and Selective Laser Processing-A Computational Manufacturing Framework," Comput. Mech., **54**(1), pp. 171–191.
[7] Zohdi, T. I., 2015, "Modeling and Simulation of Cooling-Induced Residual Stresses in Heated Particulate Mixture Depositions," Comput. Mech., **56**(4), pp. 613–630.
[8] Kruth, J., Levy, G., Schindel, R., Craeghs, T., and Yasa, E., 2008, "Consolidation of Polymer Powders by Selective Laser Sintering," International Conference on Polymers and Moulds Innovations, Ghent, Belgium, September.
[9] Bertrand, P., Bayle, F., Combe, C., Goeuriot, P., and Smurov, I., 2007, "Ceramic Components Manufacturing by Selective Laser Sintering," Appl. Surf. Sci., **254**(4), pp. 989–992.
[10] Kinstlinger, I. S., Bastian, A., Paulsen, S. J., Hwang, D. H., Ta, A. H., Yalacki, D. R., Schmidt, T., and Miller, J. S., 2016, "Open-Source Selective Laser Sintering (opensls) of Nylon and Biocompatible Polycaprolactone," PLoS One, **11**(2), pp. 1–25.

[11] Oñate, E., Idelsohn, S. R., Celigueta, M. A., and Rossi, R., 2008, "Advances in the Particle Finite Element Method for the Analysis of Fluid Multibody Interaction and Bed Erosion in Free Surface Flows," Comput. Methods Appl. Mech. Eng., **197**(19–20), pp. 1777–1800.
[12] Oñate, E., Celigueta, M. A., Idelsohn, S. R., Salazar, F., and Suárez, B., 2011, "Possibilities of the Particle Finite Element Method for Fluid-Soil-Structure Interaction Problems," Comput. Mech., **48**(3), pp. 307–318.
[13] Oñate, E., Celigueta, M. A., Latorre, S., Casas, G., Rossi, R., and Rojek, J., 2011, "Lagrangian Analysis of Multiscale Particulate Flows With the Particle Finite Element Method," Comput. Part. Mech., **1**(1), pp. 85–102.
[14] Carbonell, J. M., Oñate, E., and Suárez, B., 2010, "Modeling of Ground Excavation With the Particle Finite Element Method," J. Eng. Mech., **136**(4), pp. 455–463.
[15] Labra, C., and Oñate, E., 2009, "High-Density Sphere Packing for Discrete Element Method Simulations," Commun. Numerical Methods Eng., **25**(7), pp. 837–849.
[16] Rojek, J., Labra, C., Su, O., and Oñate, E., 2012, "Comparative Study of Different Discrete Element Models and Evaluation of Equivalent Micromechanical Parameters," Int. J. Solids Struct., **49**(13), pp. 1497–1517.
[17] Rojek, J., 2014, "Discrete Element Thermomechanical Modeling of Rock Cutting With Valuation of Tool Wear," Comput. Particle Mech., **1**(1), pp. 71–84.
[18] Avci, B., and Wriggers, P., 2012, "A DEM-FEM Coupling Approach for the Direct Numerical Simulation of 3D Particulate Flows," ASME J. Appl. Mech., **79**(1), p. 010901.
[19] Leonardi, A., Wittel, F. K., Mendoza, M., and Herrmann, H. J., 2014, "Coupled DEM-LBM Method for the Free-Surface Simulation of Heterogeneous Suspensions," Comput. Particle Mech., **1**(1), pp. 3–13.
[20] Bolintineanu, D. S., Grest, G. S., Lechman, J. B., Pierce, F., Plimpton, S. J., and Schunk, P. R., 2014, "Particle Dynamics Modeling Methods for Colloid Suspensions," Comput. Particle Mech., **1**(3), pp. 321–356.
[21] Salloum, M., Johnson, K. L., Bishop, J. E., Aytac, J. M., Dagel, D., and Waanders, B. G. V. B., 2019, "Adaptive Wavelet Compression of Large Additive Manufacturing Experimental and Simulation Datasets," Comput. Mech., **63**(3), pp. 491–510.
[22] Huang, Y., Leu, M. C., Mazumdar, J., and Donmez, A., 2015, "Additive Manufacturing: Current State, Future Potential, Gaps and Needs, and Recommendation," ASME J. Manuf. Sci. Eng., **137**(1), p. 014001.
[23] Okada, T., Ishige, R., and Ando, S., 2016, "Analysis of Thermal Radiation Properties of Polyimide and Polymeric Materials Based on ATR-IR Spectroscopy," J. Photopolym. Sci. Technol., **29**(2), pp. 251–254.
[24] Mark, J. E., 1999, *Polymer Data Handbook*, Oxford University Press, New York.
[25] Sartori, E., 2006, "Convection Coefficient Equations for Forced Air Flow Over Flat Surfaces," Solar Energy, **80**(9), pp. 1063–1071.
[26] Millot, C., Fillot, L. A., Lame, O., Sotta, P., and Seguela, R., 2015, "Assessment of Polyamide-6 Crystallinity by DSC: Temperature Dependence of the Melting Enthalpy," J. Therm. Anal. Calorim., **122**(1), pp. 307–314.
[27] Zohdi, T. I., 2006, "Computation of the Coupled Thermo-Optical Scattering Properties of Random Particulate Systems," Comput. Methods Appl. Mech. Eng., **195**(41–43), pp. 5813–5830.
[28] Gross, H., 2005, *Handbook of Optical Systems. Fundamental of Technical Optics*, Wiley-VCH, Weinheim.
[29] Ganeriwala, R., and Zohdi, T. I., 2016, "A Coupled Discrete Element-Finite Difference Model of Selective Laser Sintering," Granul. Matter, **18**(2).
[30] Zohdi, T. I., 2013, "Rapid Simulation of Laser Processing of Discrete Particulate Materials," Arch. Comput. Methods Eng., **20**(4), pp. 309–325.
[31] Zohdi, T. I., 2018, "Construction of a Rapid Simulation Design Tool for Thermal Responses to Laser-Induced Feature Patterns," Comput. Mech., **62**(3), pp. 393–409.
[32] Zohdi, T. I., 2018, "Laser-Induced Heating of Dynamic Depositions in Additive Manufacturing," Comput. Methods Appl. Mech. Eng., **331**(1), pp. 232–258.